PAPER

Electrohydrodynamic (EHD) jet printing with a circulating dual-channel nozzle

IOP Publishing Journal of Micromechanics and Microengineering
J. Micromech. Microeng. 29 (2019) 035013 (10pp) https://doi.org/10.1088/1361-6439/aafd9e

Electrohydrodynamic (EHD) jet printing with a circulating dual-channel nozzle

Zhen Li, Karam Nashwan Al-Milaji, Hong Zhao and Da-Ren Chen

Department of Mechanical and Nuclear Engineering, Virginia Commonwealth University, Richmond, VA, United States of America

E-mail: dchen3@vcu.edu and hzhao2@vcu.edu

Received 4 August 2018, revised 17 October 2018
Accepted for publication 7 January 2019
Published 31 January 2019

Abstract

Electrohydrodynamic (EHD) printing is a promising technique for additive manufacturing of high-resolution features with low cost and high efficiency. One of the major issues in EHD printing is nozzle clogging, which often occurs in the printing of colloidal inks with high concentrations. We proposed a new EHD printing nozzle configuration with dual channels to enable ink flow circulation to resolve the above issue. In this study, we focused on the meniscus dynamics and jetting characteristics of this new EHD printing process. Various jetting modes, i.e. continuous jet, pulsating jet, and pulsating droplet, as a function of the electric field intensity and nozzle configuration, were discussed. Dot patterns on a flexible substrate have been demonstrated via the new EHD printing process when operated at the pulsating droplet mode.

Keywords: electrohydrodynamic (EHD) printing, dual-channel, ink circulation, meniscus dynamics

Supplementary material for this article is available online

(Some figures may appear in colour only in the online journal)

1. Introduction

As an emerging inkjet printing technology, electrohydrodynamics (EHD) printing has been demonstrated to fabricate micro/nano-scaled patterns/features because of its high resolution, good compatibility with a variety of inks and substrates, and all of the attributes of conventional inkjet printing (e.g. direct-write process, potential to integrate into a roll-to-roll manufacturing process, ambient operation, etc) [1–7]. As a result, EHD printing has attracted extensive research interests and has been successfully applied for direct 2D and 3D fabrication of micro/nano-scaled structures in applications, e.g. micro-electronics [8–11], pharmaceutics [12, 13], patterning of biomolecules [14–16], fabrication of functional materials with polymers, metal nanoparticles, and biologic materials [17–20].

Different from the conventional inkjet printing, ink droplets (or jets) in an EHD jet printing are pulled out (rather than being pushed out) from the droplet-emitting opening of a printing nozzle by an external electric field. During the EHD printing, the shape of ink meniscus at the droplet-emitting opening of the printing nozzle changes when an electric field is established between the printing nozzle tip and substrate. The resultant meniscus shape depends on the balance among surface tension, electrostatic force, and hydrostatic pressure [21–23]. In all of the previous literature regarding the EHD printing [24–27], single-capillary nozzles have been exclusively used to generate ink droplets. When a high electric field is established between the nozzle and substrate, the liquid meniscus pinned at the tip of the capillary deforms from the semi-spherical shape into a conical shape. A jet (or filament) emits from the cone tip and ink droplets form once the jet breaks up. The cone-shaped meniscus retracts to its original shape after the applied electric field is off. The neck-down ratio (i.e. the nozzle inner diameter (ID), versus droplet diameter) in the EHD printing is typically by a factor of 10 or less [28, 29].

For the above reason, fine nozzles with IDs of several micrometers were used to generate micro or sub-micro patterns/features by the single-capillary EHD printing. The IDs

of the capillary nozzles have been reduced from several hundred micrometers (in a typical electrospray system) down to 1–2 μm or even less than 1 μm in the majority of the single-capillary EHD printing studies. As the nozzle size scales down, it is inevitable to encounter severe nozzle clogging. For printing functional inks including colloidal suspensions, agglomeration of primary particles often results in the nozzle clogging, induced by the heterocoagulation of micrometer-sized agglomerates. The clogging can also be induced either by the shear-induced gelation in liquid-like colloidal suspensions or hydrodynamic bridging [30–32]. This may occur when several particles simultaneously arrive at the emitting end of the single capillary nozzles even when the sizes of primary particles are smaller by one order of magnitude than the nozzle opening diameter. Another mechanism for nozzle clogging is due to solvent evaporation and/or ink polymerization during the printing. Thus, extremely diluted inks were usually used in the current EHD printing [32, 33], which adversely impacted the quality of the printed features and throughput.

In this work, we introduced a new dual-channel printing nozzle, which enables a circulating ink path, to prevent the nozzle from clogging. During the nozzle operation, ink is continuously injected into the nozzle through one flow channel and extracted from the other. A stable ink meniscus is established at the emitting opening of the nozzle, where the ink bridges the two channels. When an electric field is applied between the nozzle and the substrate, the ink meniscus is activated and one single droplet (or a jet) may be ejected. The unconsumed ink is continuously circulated. The issue of nozzle clogging associated with ink polymerization or solvent evaporation at the droplet-emitting opening in the single-capillary nozzle can be greatly suppressed by keeping the printing ink moving as demonstrated in figure S1 in the supporting information (stacks.iop.org/JMM/29/035013/mmedia). Because of the unique nozzle design, the jetting characteristics and meniscus dynamics are expected to be different from those in the conventional single-capillary EHD printing. In this study, we identified and discussed various jetting modes in this new EHD printing process under different pulse voltage settings applied between the nozzle and substrate. The effects of the applied electric field and ink properties on the jetting onset and droplet size were further investigated. Dot patterns were demonstrated via the use of this new dual-channel EHD printing.

2. Experimental method

The dual-channel EHD nozzle is composed of mainly two parts. One is the supporting body known as the outer channel (ID = 457 μm) that is used to fix the capillaries coaxially, and the other is the capillary known as the inner channel (ID = 203 μm). It is challenging to maintain the concentricity of the capillary due to the small size of the diameters. The supporting body structure used an axial multi-lumen/channel tube. The capillary was positioned in the central hole, ensuring accurate coaxial alignment of the capillary with the outer channel of the supporting body. Therefore, the concentricity was achieved by creating and leveraging six proper constraint points.

The electrical power supply in the setup comprised a high-voltage amplifier (Matsusada, AMT-20B10-LCN1) used to establish a high electric field between the printing nozzle and substrate for EHD printing. A function generator (Fluke, Model 282) was used to provide the input for the high-voltage amplifier to generate various printing sequences. The amplitude and frequency of the printing sequences were monitored by an oscilloscope (Agilent, 54622A). The deposition substrate was mounted on an *X*-*Y* moving stage, and its motion was driven by two high-resolution linear motors (Thorlabs, MTS25-Z8). The optical system that monitored the dynamics of ink meniscus at the droplet-emitting opening of the dual-channel EHD printing nozzle consisted of a high-speed camera (Phantom, Miro 3a10), a microscopic lens (InfiniVar CFM-2/S), and a LED light source. The feeding and extraction of printing ink from the dual-channel EHD nozzle was carried out by two syringe pumps (Harvard PHD2000, Harvard Inc.).

Mixtures of oleic acid (OA) and isopropanol (IPA) (Sigma Aldrich) were used as the inks in this study. The surface tension and viscosity of the printing inks varied by the volume ratio of OA and IPA. The ink surface tension was characterized on a goniometer (OCA 15, DataPhysics) using pendant drop method. The ink conductivity was measured by a conductivity meter (Thermo Fisher, Model Orion STAR A215). The surface tension and conductivity measurements have been repeated three times for each ink solution.

Fluorescein sodium salt (Sigma-Aldrich, F6377) was dissolved in the solution mixture of OA and IPA with a concentration of ~42.0 mg ml^{-1}. The printed dot patterns were imaged by a fluorescent microscope (AmScope, 40× –1000×). The dot diameter on the PET substrate and the standard deviation were obtained by averaging over ~50 dots.

3. Results and discussion

3.1. Design of dual-channel EHD printing nozzle

Figure 1(a) shows the schematic diagram of the dual-channel EHD printing nozzle with a circulating ink path. The dual-channel printing nozzle was constructed by the assembly of two coaxially aligned capillaries. Ink flow passes through the inner channel and circulates back through the outer channel (i.e. the annular spacing between inner and outer capillaries). The inner capillary tip slightly protrudes beyond the end of the outer capillary, where ink meniscus is formed and pinned. When the ink climbs the outer surface of the inner capillary and reaches the end of the outer capillary, a 'liquid bridge' is established between the inner and the outer channels with the ink flowing in the free space in-between.

The experimental setup for the dual-channel EHD printing is illustrated in figure 1(b). The setup consisted of an open-loop ink-flow control system, a voltage supply, a linear moving stage, and an optical system to capture the meniscus images. The ink-flow control system included two syringe pumps with

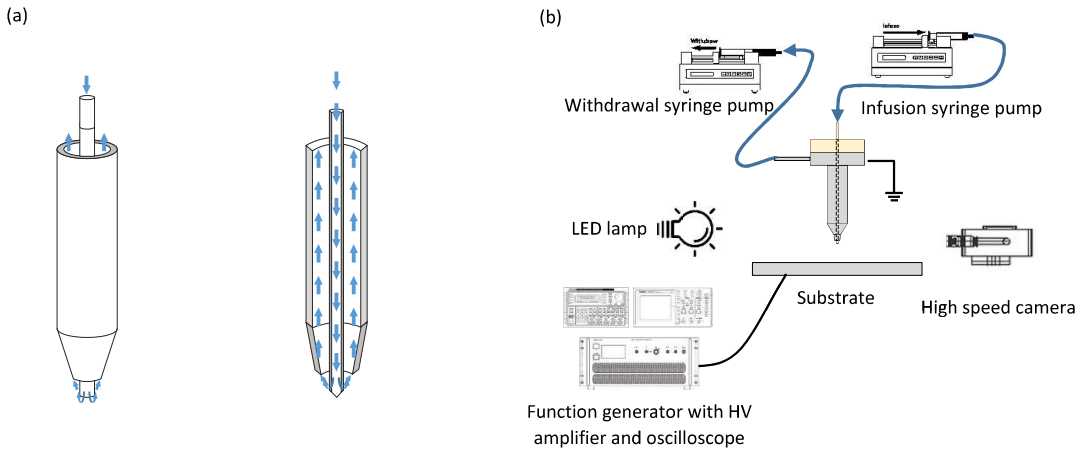

Figure 1. Schematic diagrams of (a) the dual-channel nozzle with the circulating ink path, and (b) the experimental setup to study the dual-channel EHD printing.

infusion and withdrawal capabilities, which continuously injected ink into the inner channel of the dual-channel EHD nozzle. This was done by the infusion syringe pump while the withdrawal syringe pump extracted the unconsumed ink through the outer channel. The voltage supply consisted of a function generator, a voltage amplifier and an oscilloscope. The voltage was directly applied on the substrate, while the printing nozzle was on the electrical ground. By establishing an electric field between the nozzle and the substrate, the ink meniscus is deformed into a cone, ejecting either one single droplet or a thin filament from the cone tip (section 3.3). A high-speed camera with a microscopic lens was used to monitor the formation of meniscus and its subsequent transition into either a jet or a droplet.

3.2. Continuous ink circulation

When the inner ink injection has the same flow rate as the outer ink withdrawal, a 'stationary' and stable meniscus is established at the tip of the inner capillary, connecting to the outer channel through a liquid bridge and circulating without any air bubbles. However, solvent evaporation from the meniscus at room temperature causes ink loss. Therefore, the ink withdrawing flowrate needs to be smaller than the feeding flowrate to compensate for the evaporation loss. Otherwise, the liquid bridge between the inner and outer breaks and disconnects, leading to a conventional single-capillary inkjet printing. Δflowrate, i.e. the difference between the injecting flowrate and withdrawing flowrate, was chosen from 0.5 μl min^{-1} (the minimal Δflowrate) to 1.5 μl min^{-1} (the maximal Δflowrate) to avoid ink accumulation at the tip of the nozzle.

Initial experiments were performed to identify the lower and upper limits of applied voltage under a given Δflowrate, at which a stable cone-jet forms and circulates continuously. The pure IPA, with a conductivity of 11.9 μS cm^{-1}, was employed in this study. In this case, a constant DC voltage was applied to the substrate and an electric field was generated between the capillary tip and the substrate. The lower boundary voltage represents the threshold voltage when a cone shape of the meniscus is produced and ink is ejected. As shown in figure 2(a), the voltage decreases as the Δflowrate increases. It suggests that the higher the Δflowrate is, the easier the cone-jet mode formation will be. Since the additional ink supplied leads to a larger volume of a pendant droplet, the forefront of the meniscus gets closer to the substrate. Thus, the meniscus deforms into a cone shape relatively easier for a given voltage. The upper boundary voltage represents the critical voltage when the electric field deforms the meniscus to an extent that the liquid bridge between the two channels is broken, thereby causing failure of ink circulation. As the Δflowrate increases, the upper boundary voltage remains fairly constant. For a given inner nozzle extension, only the volume of the pendant ink below the inner nozzle tip is influenced by the Δflowrate, while the volume of the liquid bridge stays relatively the same. The critical voltage of the bridge breakdown will be more or less constant for a given bridge volume, which is determined mostly by the inner nozzle extension length. As the extension length decreases, both the upper boundary and lower boundary voltages increase due to the change of the meniscus volume and shape. It is indicated that the volume decrease of the ink bridge between the inner and outer nozzles, as well as the less sharp curvature of the meniscus, can significantly reduce the risk of liquid bridge breakdown. A small amount of the ink bridge exposure to high electric field is expected to undergo less influence on its stability.

To study the jetting characteristics for the dual-channel nozzle, the extension length of 0.24 mm was selected for the following experiment due to its wider operation window. For the printing inks with different conductivities, the relationship of Δflowrate and voltage boundary is shown in figure 2(b). The critical voltage shows the same general trend with the Δflowrate. As ink conductivity increases, both the lower and upper boundaries decrease. Under the same voltage condition, operation at high conductivity results in a corresponding high rate of ink consumption. For that reason, the meniscus bridge could easily reach the upper voltage limit. On the other hand, the lower voltage threshold decreases since high conductivity favors the jet formation. It is worth noting that a

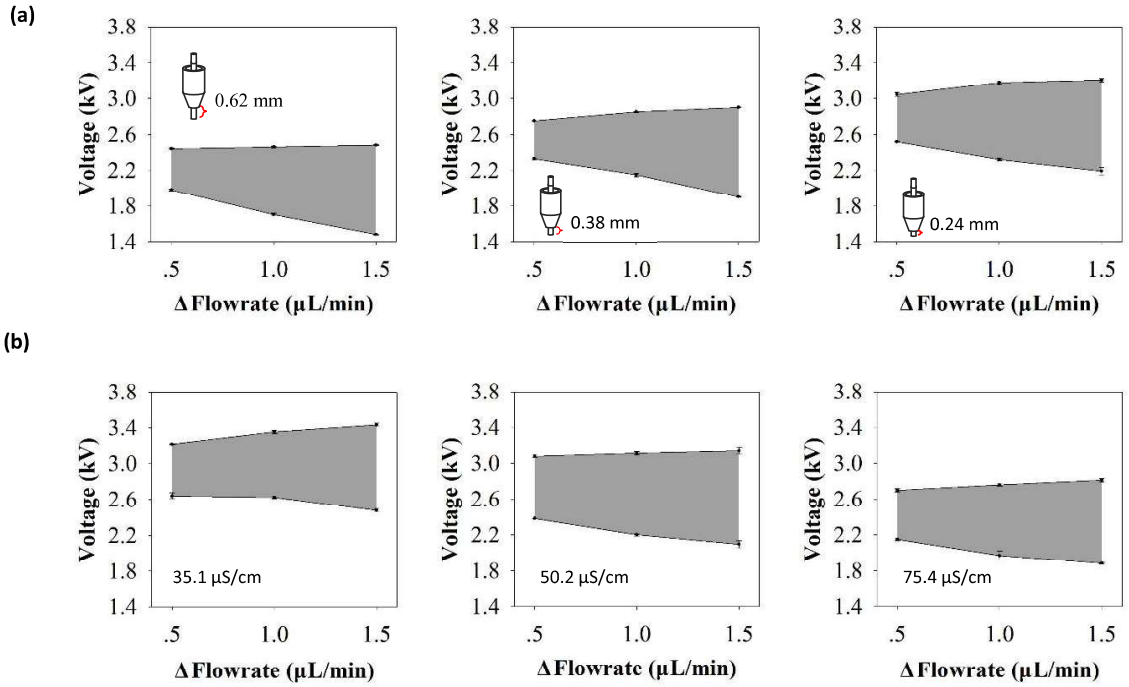

Figure 2. Voltage requirement for a steady circulation between the inner and outer channels (a) for various inner nozzle extensions (the pure IPA with a conductivity of 11.9 μS cm^{-1} was used), (b) for IPA inks with different conductivities. The shortest inner nozzle extension was used.

dynamic voltage, i.e. a pulsed voltage superposed on an offset DC voltage (instead of the constant DC voltage in figure 2), was applied to produce the on-demand droplets in sections 3.3–3.5. Although the critical voltage for steady circulation is different from the dynamic voltage, the principle of how the voltage affects the formation of steady circulation and its subsequent breakdown has held true. We hypothesized that for a given inner capillary extension length and flowrate, the critical voltage for the dynamic voltage could be a little higher, due to the significant shorter duration than the stable DC voltage.

3.3. Jetting modes for dual-channel EHD printing

For on-demand ink deposition and pattern generation, the pulse voltage operation has been evidenced more suitable in the EHD printing [34]. In this work, we applied a dynamic voltage on the substrate by superposing a pulse voltage on an offset DC voltage. The offset DC voltage could be considered as a base voltage to ease the meniscus transition from the hemispherical shape into a conical one. The applied offset voltage also provides an additional driving force to accelerate the droplet/filament toward the substrate. Three jetting modes, i.e. continuous jet, pulsating jet, and pulsating droplet, were identified in this dual-channel EHD printing.

3.3.1. Continuous jet mode. In the continuous jet mode (figures 3(a) and (d)), a sharp conical meniscus with a thin jet emits from its apex. In this mode, the shape of the ink meniscus does not change to the conical shape until ~1.4 ms after the pulsed voltage is on. Once the meniscus shape changes, a liquid jet gradually protrudes from the cone tip in the direction of the electric field. The jets eventually break into a spray of droplets. Despite the fact that the pulse voltage is turned off, the jetting continues, maintaining its shape for a brief period of time (~2.2–2.4 ms) followed by meniscus retraction. The above sequence repeats in additional cycles of applying the pulse voltage.

3.3.2. Pulsating jet mode. The pulsating jet mode was observed by increasing the magnitude of either the pulse voltage or the offset DC voltage. In the pulsating jet mode, the shape of the ink meniscus deforms from the semi-spherical shape to a conical one. A thin thread/filament emits from the cone apex. Note that the difference between the pulsating jet and continuous jet modes lies in the shape of the cone apex. In the pulsating jet mode, a thin liquid thread that is confined at the apex quickly pinches off from the conical meniscus at the end of the applied pulse voltage. Due to the inertial and electrical forces, the pinched-off liquid thread travels toward the substrate and deposits on the substrate. At the same time, the conical meniscus retracts to its original shape (figures 3(b) and (e)) once the strength of the offset DC voltage is insufficient to deform the ink meniscus. The pulsating jet mode has been reported in other single-capillary EHD printing studies [4, 35]. In the work of Lee *et al* [36], a jet appeared in a few milliseconds (~0.5 ms) after the start of the pulse voltage cycle and the jetting was repeated several times in the pulse duration. In this study, the jet pulsating occurs only once during one pulse cycle and presents at the end of the voltage pulse duration. The ink ejection is initiated by the deformation of

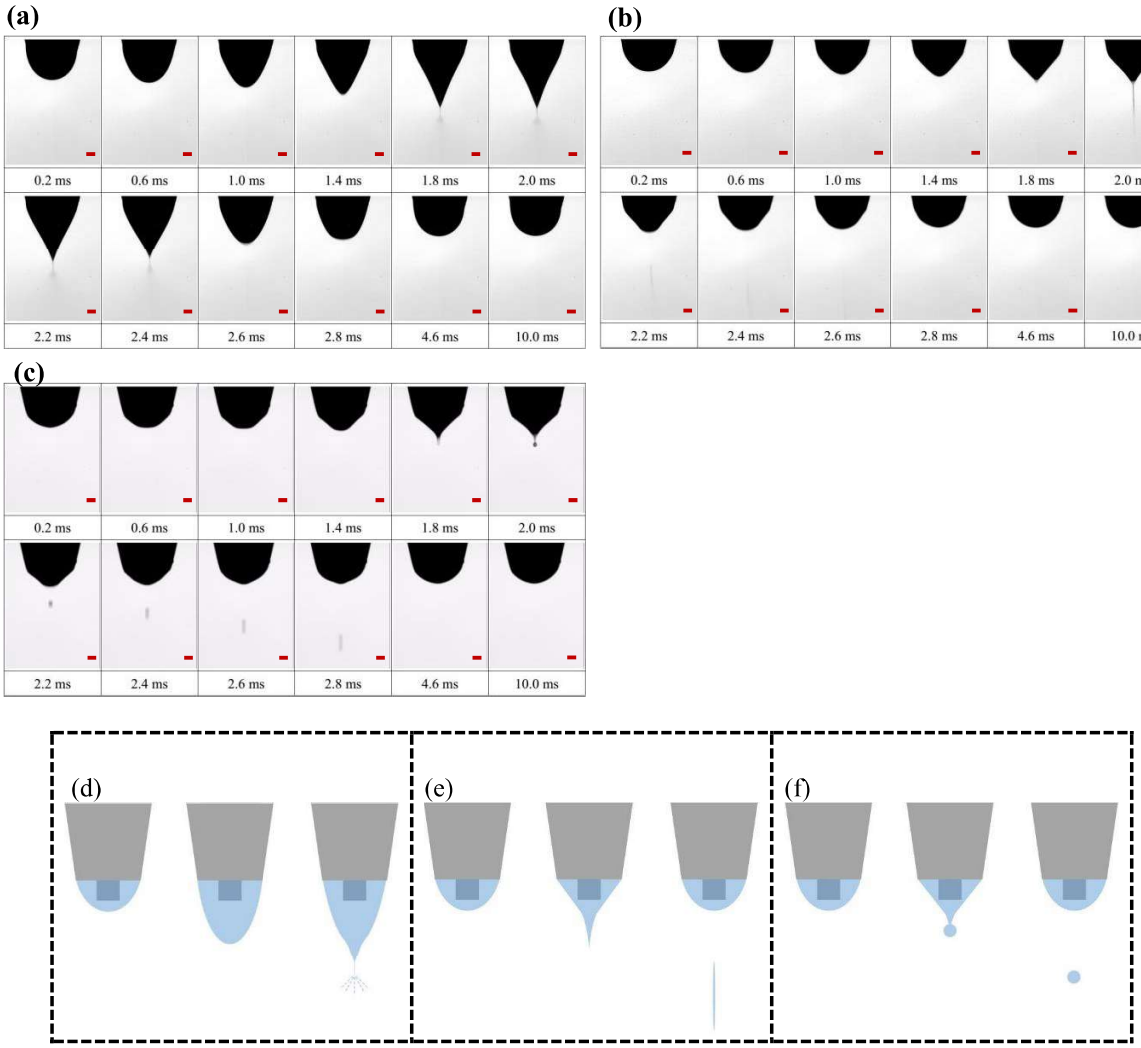

Figure 3. Time-resolved images of three jetting modes: (a) continuous jet, (b) pulsating jet, and (c) pulsating droplet. Scale bars are 200 μm. (d)–(f) Schematics of the three jetting modes. The ink consists of 20% OA and 80% IPA with a conductivity of 22.0 μS cm^{-1}. Pulse duration is 2 ms.

ink meniscus, which is essentially determined by the electrical property of the printing ink, and their electro- and hydrodynamic- interactions with the applied electric field. The rate of ink meniscus deformation is related to the hydrodynamic relaxation and charge relaxation times [37]. The characteristic hydrodynamic relaxation time is typically much longer than the charge relaxation time [35], especially for low-conductivity inks. It is possible that the pulse duration of 2 ms is greater than the charge relaxation time, but less than the hydrodynamic relaxation time, resulting in one pinched-off filament in one pulse cycle. In fact, multiple jets in one pulse cycle does exist when printing highly conductive inks with a long pulse duration (e.g. 4 ms) (figure S2 in the supporting information). Due to the fact that one jet in one pulse cycle is desirable for producing stable dots via EHD printing, multiple-jet mode was not further explored in this work.

3.3.3. Pulsating droplet mode. In the pulsating droplet mode, a high pulse voltage is required to pull the ink from the cone apex to form a droplet. The ink at the apex of the conical liquid meniscus maintains its spherical shape rather than becomes a thread in the pulsating jet mode (figures 3(c) and (f)). The droplet connects to the apex of conical ink meniscus for a very short period prior to its pinch-off. A thin ink filament is often observed after the droplet pinches off and eventually forms a satellite droplet with a diameter smaller than that of the primary droplet. The size of satellite droplets increases as the ink filament stretches. The ink filament pinches off from the meniscus apex when the pulse voltage is switched off. In the optimum conditions, clean pinch-off can be obtained without satellite droplet formation.

The combination of a high pulse voltage with a low offset DC voltage is prone to produce a droplet at the apex of the

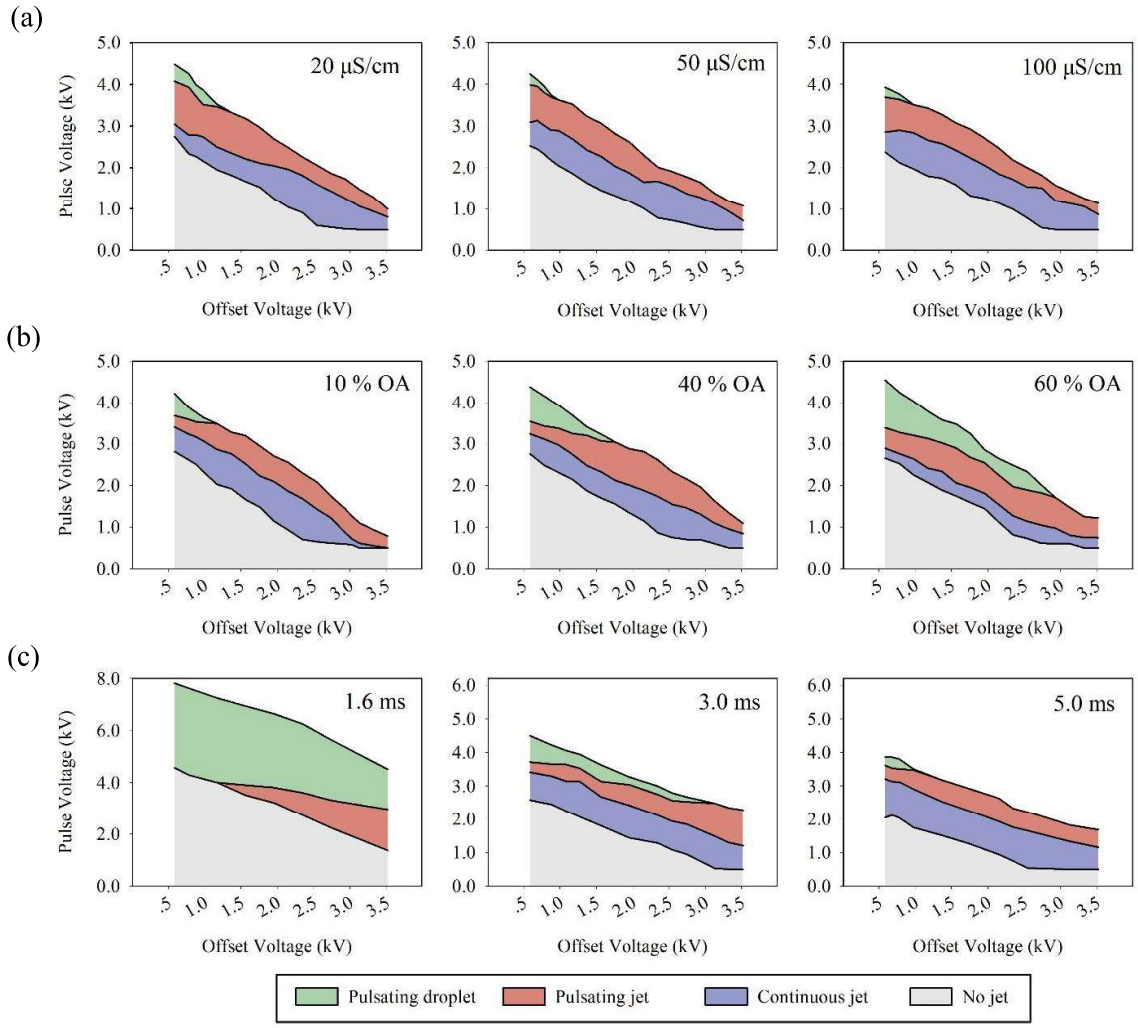

Figure 4. Jetting mode domains for inks (a) with different conductivities, and (b) with different viscosities, under a constant pulse duration of 4 ms, and (c) with different pulse durations (40% OA and conductivity of 20 μS cm^{-1} were used).

liquid cone during the meniscus deformation. The low offset DC voltage is insufficient to deform the droplet into a thread. At a high offset DC voltage, ink meniscus in the near-cone shape has been achieved prior to the application of the pulse voltage. It is thus difficult for the subsequent pulse voltage to produce a droplet via the meniscus deformation.

3.4. Domains of various jetting modes

Figure 4(a) shows the domains of various jetting modes for printing OA-IPA mixtures as a function of the applied electric field. The OA percentage (20% volume) remains the same. For a given offset DC voltage and a given electrical conductivity, the continuous jet mode is firstly obtained and then followed by the pulsating jet and pulsating droplet modes as the pulse voltage increases. As the offset DC voltage increases, the maximum pulse voltage maintaining steady ink circulation decreases. Once exceeding the maximum pulse voltage, the ink bridge of the two flow channels breaks and the ink circulation has been no longer possible. This makes the dual-channel EHD printing the same as a single-capillary printing.

As shown in figure 4(a), the increase in electrical conductivity of OA-IPA mixtures decreases the threshold pulse voltage needed for jetting to occur. Under the same offset DC voltage, the pulsating droplet mode is difficult to obtain when printing highly conductive OA-IPA inks. More mobile ions available in the highly conductive inks facilitate the thread formation under the applied electric field. A detailed comparison of the boundaries of various jetting modes is provided in figure S3 (supporting information).

As the percentage of OA increases (figure 4(b)) and the viscosity of the OA-IPA mixture increases, the domains of various jetting modes change notably. The ink conductivity of 20 μS cm^{-1} remains the same. It is worth pointing out that, although the OA/IPA ratio was varied to prepare printing inks with different viscosities, the surface tensions of the printing inks are in fact very close, i.e. 21.06–22.62 mN m^{-1} (table S1). As the percentage of OA increases in the printing inks,

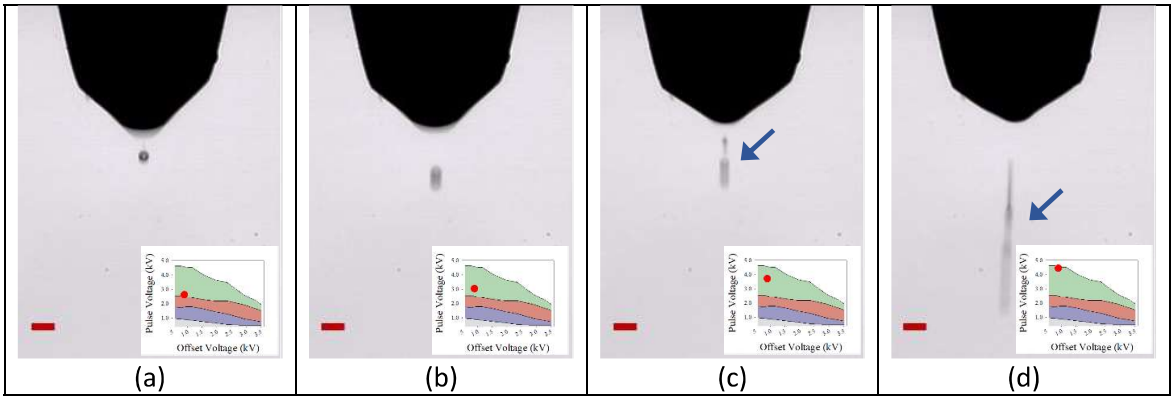

Figure 5. Images of droplet formation at the pulsating droplet mode under conditions of different pulse voltages: (a) 4.30 kV, (b) 4.69 kV, (c) 5.08 kV, and (d) 5.48 kV. Scale bars are 200 μm. The mixture of 40% OA and 60% IPA with a conductivity of 20 μS cm^{-1} was used. The inset shows the domains of the jetting modes. The red dot shows the pulse voltage setting and its corresponding position in the pulsating droplet domain. The arrow refers to the non-spherical droplet formation.

the domain of the pulsating droplet mode widens. A high percentage of OA facilitates the droplet formation due to its high viscosity. More viscous ink prompts the easy formation of long liquid filament at the apex of the conical meniscus. It can be further noted that, as the OA content in the printing inks increases, the ink filament is more stable during the voltage pulse. Once the ink accumulates to a certain volume, the ink filament would eventually pinch off from the conical meniscus when the voltage pulse is off.

In contrast, the domain of continuous jet mode decreases as the viscosity of the OA-IPA mixture increases. The lower and upper boundaries of the pulse voltage for maintaining the continuous jet mode also decreases. However, the onset voltage for the continuous jet mode does not show a notable difference for any of the studied inks. This might be attributed to the similar surface tensions of those inks.

Figure 4(c) shows the various jetting modes at different pulse durations of 1.6 ms, 3 ms and 5 ms, respectively. The relative arrangement of the domains of each jetting mode is similar to figures 4(a) and (b), but with different domain sizes. At the shortest pulse duration (1.6 ms), the domain of the continuous jet mode disappears and the pulsating jet mode has not been observed when the offset voltage is lower than 1.2 kV. The disappearance of the continuous jet mode is presumably due to the fact that the time required for the formation of a continuous jet is longer than the set pulse duration. From another perspective, it is difficult to develop a continuous jet mode which would automatically transition into a pulsating jet mode (or droplet mode) that is more likely to separate from the meniscus within such a short pulse duration. As the offset voltage increases, the pulsating jet mode presents. The domain of the pulsating droplet mode is significantly larger in the shorter pulse condition. Due to the short pulse duration, a higher voltage is required to produce the droplet mode. The neck length between the droplet and the meniscus may be short and maybe difficult to stretch the droplet, which promotes the formation of droplet. The upper boundaries of the pulse voltage have significantly increased. When the offset voltage is 0.49 kV, the upper boundary of the voltage is close to 8.0 kV which is significantly higher than that of any other conditions in this study. Due to the short pulse time, deformation of the meniscus is also decreased in order to maintain the ink bridge. The increase in pulse duration actually decreases the initial voltage and increases the domain of continuous jet mode concurrently with the shrinkage of the domain of the droplet mode. The pulse duration is long enough to accumulate the ink while deforming and stretching it, thus increasing the domain of continuous jet mode. When the pulse duration increases to 5 ms, the droplet mode only exists when a low offset voltage is applied. In addition, as the offset voltage increases, high voltage allows enough deformation time for the meniscus and decreases the upper boundary of the pulse voltage. Figure S3 compares the voltage boundaries for each jetting mode.

3.5. Dot patterns by dual-channel EHD printing

We have printed the dot patterns on the substrate of coated polyethylene terephthalate (PET). In this study, the coated PET substrate was used to eliminate the effect of substrate wettability. When the nozzle operates at the pulsating jet mode (figures 3(b) and (e)), some part of the charged thread-shaped jet may break down into tiny satellites or sprays. For that reason, it is considered that the pulsating droplet mode is the more appropriate operating condition for EHD printing with the dual-channel nozzle apparatus.

For a specific ink formulation, the jetting mode depends on the offset DC voltage, pulse voltage, and pulse duration (figure 4). The offset DC voltage works as a base voltage to facilitate the meniscus transition from the spherical cap shape into a conical one. Furthermore, it also provides the main driving force to accelerate the ejected droplet towards the substrate. When a pulse voltage is applied to the liquid meniscus, it is superposed on the offset voltage to create the jetting. For the pulsating droplet mode, a higher effective voltage (i.e. superpose of the offset voltage and the pulse voltage), not only results in a larger droplet volume but also influences the droplet shape. Therefore, the operating zone of pulsating

droplet mode in the phase diagram in figure 4 does not guarantee a perfect spherical droplet formation. Figure 5 shows the droplet formation under conditions of different pulse voltages. For each condition, the pulse duration (1.8 ms) and offset voltage (1.56 kV) remain unchanged. A nearly perfect spherical droplet is formed at a lower pulse voltage (figure 5(a)). The charged droplet tends to preserve its shape as it travels toward the substrate in the presence of the offset voltage. Deposition of uniform dots with circular shape is obtained on the PET substrate. As the pulse voltage increases, the droplet deforms into an ellipse shape. Although the offset voltage (1.56 kV) is much lower than the pulse voltage (4.69 kV), the droplet has been elongated while travelling (figure 5(b)). It appears as a dot when the droplet deposits onto the substrate. At higher pulse voltages (figures 5(c) and (d)), the droplets are deformed to a greater extent so that the droplets tend to fall apart. The ink is distributed non-uniformly within the droplet leading to further falling apart during travelling. Figures 5(c) and (d) correspond to jetting conditions of non-spherical droplet formation while they still belong to the pulsating droplet mode. When the non-spherical droplets deposit onto the substrate, the printed dots present irregular shapes and satellites, since the greatly deformed droplets are not able to travel exactly along the same path. Therefore, without optimized pulse durations, uniform dot patterns with a circular shape can hardly be achieved at high pulse voltages.

For this reason, the pulse duration was fine-tuned (slightly decreasing) as the pulse voltage increasing in order to ensure good droplet formation without satellites. Figure 6(a) shows the dot size as a function of pulse voltage when the nozzle operates at the pulsating droplet mode. Figure 6(b) presents optical images of the dot patterns obtained in figure 6(a). The dot size decreases from 229.75 $\pm$ 7.18 μm to 134.15 $\pm$ 5.62 μm gradually as the pulse voltage decreases from 5.38 to 4.23 kV, and the offset voltage remains the same (0.89 kV). The above observation indicates the monotonic correlation of droplet size with the pulse voltage. The pulse duration needs to be sufficiently long to eject the droplet but not too long to induce shape deformation. With non-optimized pulse durations, the printed dots exhibit irregular shapes and satellites near the main dots (figure S4 in the supporting information). Therefore, both the pulse voltage magnitude and duration influence the jetted droplet volume (and dot size correspondingly) and the deposited dot quality. As evident in figure 6(a), the dot size could be decreased via the decrease of the pulse voltage magnitude, with an optimal setting of the pulse duration to obtain uniform dots of small size when operated under the pulsating droplet mode.

It is worth noting that the offset DC voltage contributes to meniscus deformation before reaching the conical shape, as well as the droplet transport in the electric field. Deflection could occur during the droplet transport to the substrate when a low offset voltage is applied. Gravity is less significant for the droplets in the current size range since the Bond number (Bo) is much less than 1.

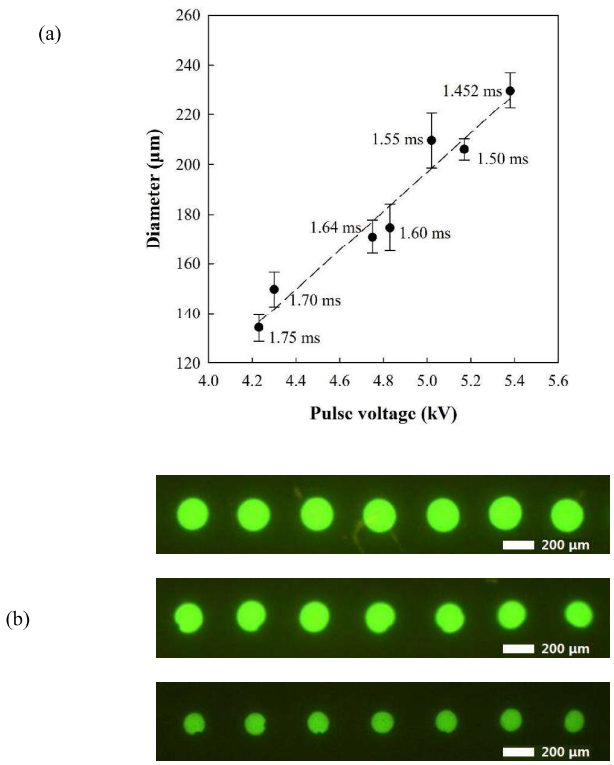

Figure 6. (a) Dot diameter versus pulse voltage at the pulsating droplet mode. The pulse duration for each data point is attached. The mixture of 40% OA and 60% IPA with a conductivity of 20 μS cm^{-1} was used. Offset DC voltage was kept at 0.89 kV. The pulse duration was fine tuned to maintain spherical droplet formation without satellites. (b) Images of printed dots in (a) under conditions (offset DC voltage/pulse voltage/pulse duration): 0.89 kV/5.17 kV/1.50 ms with a dot diameter of 206.05 $\pm$ 4.28 μm, 0.89 kV/4.83 kV/1.60 ms with a dot diameter of 174.75 $\pm$ 9.53 μm, and 0.89 kV/4.23 kV/1.75 ms with a dot diameter of 134.15 $\pm$ 5.62 μm, respectively.

4. Conclusion

In this work, we have demonstrated the feasibility of EHD printing via a new dual-channel nozzle and have investigated the effects of printing parameters on the meniscus dynamics and printing behavior. The dual-channel EHD printing nozzle resolves the issue of nozzle clogging, typically encountered in a single-capillary printing nozzle, by keeping the ink moving between the two channels in the nozzle.

By superposing a pulse voltage on an offset DC voltage, the dynamic voltage was applied in this EHD printing. Under different pulse voltage magnitudes and pulse durations, various jetting modes were identified, i.e. continuous jet, pulsating jet, and pulsating droplet, respectively. With a decrease in either ink conductivity or pulse duration, or an increase in the OA concentration, it is prone to produce the pulsating droplet mode and the upper boundary voltage rises. At the pulsating droplet mode, the voltages and pulse duration can be tuned

to produce spherical droplets without satellites. Dot patterns with various sizes have been demonstrated on the coated PET substrate by changing the pulse voltage and fine-tuning of the pulse duration accordingly. Further size reduction of the dual-channel printing nozzles is required in the future to realize high-resolution EHD printing. This study will lead to the development of a novel EHD jet printing technique without the primary technical barriers (e.g. nozzle clogging) and pave the way for using EHD printing as a scalable manufacturing platform.

Acknowledgments

The authors are grateful for the financial support of the National Science Foundation (NSF/CMMI 1726627) and Virginia Commonwealth University (VCU) Quest for Innovation Commercialization Fund.

ORCID iDs

Zhen Li https://orcid.org/0000-0002-8863-976X
Hong Zhao https://orcid.org/0000-0001-9148-0158

References

[1] Angmo D, Larsen-Olsen T T, Jørgensen M, Søndergaard R R and Krebs F C 2013 Roll-to-roll inkjet printing and photonic sintering of electrodes for ITO free polymer solar cell modules and facile product integration *Adv. Energy. Mater.* **3** 172–5
[2] Søndergaard R R, Hösel M and Krebs F C 2013 Roll-to-roll fabrication of large area functional organic materials *J. Polym. Sci.* B **51** 16–34
[3] Onses M S, Sutanto E, Ferreira P M, Alleyne A G and Rogers J A 2015 Mechanisms, capabilities, and applications of high-resolution electrohydrodynamic jet printing *Small* **11** 4237–66
[4] Park J-U *et al* 2007 High-resolution electrohydrodynamic jet printing *Nat. Mater.* **6** 782
[5] Kim B H *et al* 2015 High-resolution patterns of quantum dots formed by electrohydrodynamic jet printing for light-emitting diodes *Nano Lett.* **15** 969–73
[6] Singh M, Haverinen H M, Dhagat P and Jabbour G E 2010 Inkjet printing-process and its applications *Adv. Mater.* **22** 673–85
[7] Yin Z, Huang Y, Duan Y and Zhang H 2018 *Electrohydrodynamic Direct-Writing for Flexible Electronic Manufacturing* (Singapore: Springer)
[8] Baeg K J, Caironi M and Noh Y Y 2013 Toward printed integrated circuits based on unipolar or ambipolar polymer semiconductors *Adv. Mater.* **25** 4210–44
[9] Gamerith S, Klug A, Scheiber H, Scher F U, Moderegger E and List E J W 2007 Direct ink-jet printing of Ag–Cu nanoparticle and Ag-precursor based electrodes for OFET applications *Adv. Funct. Mater.* **17** 3111–8
[10] Secor E B, Prabhumirashi P L, Puntambekar K, Geier M L and Hersam M C 2013 Inkjet printing of high conductivity, flexible graphene patterns *J. Phys. Chem. Lett.* **4** 1347–51
[11] Torrisi F *et al* 2012 Inkjet-printed graphene electronics *ACS Nano* **6** 2992–3006
[12] Scoutaris N, Alexander M R, Gellert P R and Roberts C J 2011 Inkjet printing as a novel medicine formulation technique *J. Control. Rel.* **156** 179–85
[13] Niklas S, Anni M, Petri I, Leif K, Axel M, Tapani V and Jouko P 2011 Inkjet printing of drug substances and use of porous substrates-towards individualized dosing *J. Pharm. Sci.* **100** 3386–95
[14] Onses M S, Pathak P, Liu C-C, Cerrina F and Nealey P F 2011 Localization of multiple DNA sequences on nanopatterns *ACS Nano* **5** 7899–909
[15] Kim K, Lee B U, Hwang G B, Lee J H and Kim S 2010 Drop-on-demand patterning of bacterial cells using pulsed jet electrospraying *Anal. Chem.* **82** 2109–12
[16] Jayasinghe S N, Qureshi A N and Eagles P A M 2006 Electrohydrodynamic jet processing: an advanced electric-field-driven jetting phenomenon for processing living cells *Small* **2** 216–9
[17] Derby B 2010 Inkjet printing of functional and structural materials: fluid property requirements, feature stability, and resolution *Annu. Rev. Mater. Res.* **40** 395–414
[18] Hyungdong L, Baekhoon S, Jihoon K, Yonghee J and Doyoung B 2014 Direct alignment and patterning of silver nanowires by electrohydrodynamic jet printing *Small* **10** 3918–22
[19] An B W, Kim K, Kim M, Kim S Y, Hur S H and Park J U 2015 Direct printing of reduced graphene oxide on planar or highly curved surfaces with high resolutions using electrohydrodynamics *Small* **11** 2263–8
[20] Wang J-C, Zheng H, Chang M-W, Ahmad Z and Li J-S 2017 Preparation of active 3D film patches via aligned fiber electrohydrodynamic (EHD) printing *Sci. Rep.* **7** 43924
[21] Calero J F, Chato J C, Drein P T, Crowley J M and Wright G S 1988 The electrohydrostatics of a conductive liquid meniscus *Conf. Record of the 1988 IEEE Industry Applications Society Annual Meeting* (IEEE) pp 1547–51
[22] An S, Lee M W, Kim N Y, Lee C, Al-Deyab S S, James S C and Yoon S S 2014 Effect of viscosity, electrical conductivity, and surface tension on direct-current-pulsed drop-on-demand electrohydrodynamic printing frequency *Appl. Phys. Lett.* **105** 214102
[23] Jaworek A and Krupa A 1999 Classification of the modes of ehd spraying *J. Aerosol Sci.* **30** 873–93
[24] Mishra S, Barton K L, Alleyne A G, Ferreira P M and Rogers J A 2010 High-speed and drop-on-demand printing with a pulsed electrohydrodynamic jet *J. Micromech. Microeng.* **20** 095026
[25] Galliker P, Schneider J, Eghlidi H, Kress S, Sandoghdar V and Poulikakos D 2012 Direct printing of nanostructures by electrostatic autofocussing of ink nanodroplets *Nat. Commun.* **3** 890
[26] An B W, Kim K, Lee H, Kim S-Y, Shim Y, Lee D-Y, Song J Y and Park J-U 2015 High-resolution printing of 3D structures using an electrohydrodynamic inkjet with multiple functional inks *Adv. Mater.* **27** 4322–8
[27] Julian S, Patrik R, Deepankur T, Martin S, Patrick G and Dimos P 2016 Electrohydrodynamic nanodrip printing of high aspect ratio metal grid transparent electrodes *Adv. Funct. Mater.* **26** 833–40
[28] Chen C-H, Saville D A and Aksay I A 2006 Scaling laws for pulsed electrohydrodynamic drop formation *Appl. Phys. Lett.* **89** 124103
[29] Poon H F, Saville D A and Aksay I A 2008 Linear colloidal crystal arrays by electrohydrodynamic printing *Appl. Phys. Lett.* **93** 133114
[30] Xie D, Wu H, Zaccone A, Braun L, Chen H and Morbidelli M 2010 Criticality for shear-induced gelation of charge-stabilized colloids *Soft Matter* **6** 2692–8

[31] Ramachandran V and Fogler H S 1999 Plugging by hydrodynamic bridging during flow of stable colloidal particles within cylindrical pores *J. Fluid Mech.* **385** 129–56
[32] Lee A, Sudau K, Ahn K H, Lee S J and Willenbacher N 2012 Optimization of experimental parameters to suppress nozzle clogging in inkjet printing *Ind. Eng. Chem. Res.* **51** 13195–204
[33] Finn D J, Lotya M and Coleman J N 2015 Inkjet printing of silver nanowire networks *ACS Appl. Mater. Interfaces.* **7** 9254–61
[34] Paine M D, Alexander M S, Smith K L, Wang M and Stark J P W 2007 Controlled electrospray pulsation for deposition of femtoliter fluid droplets onto surfaces *J. Aerosol Sci.* **38** 315–24
[35] Bober D B and Chen C-H 2011 Pulsating electrohydrodynamic cone-jets: from choked jet to oscillating cone *J. Fluid Mech.* **689** 552–63
[36] Lee S, Song J, Kim H and Chung J 2012 Time resolved imaging of electrohydrodynamic jetting on demand induced by square pulse voltage *J. Aerosol Sci.* **52** 89–97
[37] Gañán-Calvo A M, López-Herrera J M, Rebollo-Muñoz N and Montanero J M 2016 The onset of electrospray: the universal scaling laws of the first ejection *Sci. Rep.* **6** 32357